Journal of *Marine Science and Engineering*

MDPI

Article

Simulation and Experimental Research on the Failure of Marine Sliding Bearings

Fengming Du [1], Dawei Li [1], Mingxing Hao [2], Yang Yu [3] and Weiwei Wang [4,*]

[1] College of Marine Engineering, Dalian Maritime University, Dalian 116026, China
[2] Hebei Huabei Diesel Engine Co., Ltd., Shijiazhuang 050081, China
[3] Navigation College, Dalian Maritime University, Dalian 116026, China
[4] Ocean School, Yantai University, Yantai 264005, China
* Correspondence: zhwangww@ytu.edu.cn

Abstract: The performance of the marine sliding bearing affects the reliability of marine engineering directly. Nevertheless, sliding bearings are subjected to frictional forces and problems, such as wear and fatigue, that occur after long-term use, which leads to failure. In this study, a sliding bearing friction calculation program is developed using the Fortran language, which calculates the friction force of the bearing under different working conditions. Simultaneously, a component-level sliding bearing tribology testing machine is designed, which predicts the wear failure and explores the wear mechanism for different types of sliding bearings. The model calculation results are in good agreement with the experimental data, which verifies the model's correctness. Through the wear test, the wear mechanism of the sliding bearing is mainly scratches, and the electroplating layer in the groove is squeezed out of it and attached to the surface of the aluminum alloy to reduce friction. The model and the testing machine provide theoretical guidance for the friction durability of sliding bearings used in marine engineering and guarantee the reliability of marine engineering.

Keywords: marine; sliding bearing; failure; wear; friction

Citation: Du, F.; Li, D.; Hao, M.; Yu, Y.; Wang, W. Simulation and Experimental Research on the Failure of Marine Sliding Bearings. *J. Mar. Sci. Eng.* **2023**, *11*, 61. https://doi.org/10.3390/jmse11010061

Academic Editors: Kazem Reza Kashyzadeh and Mahmoud Chizari

Received: 2 December 2022
Revised: 22 December 2022
Accepted: 24 December 2022
Published: 1 January 2023

1. Introduction

Marine engineering is becoming increasingly critical, and the stability of the power system is the premise of ensuring the normal operation of marine equipment. Sliding bearings are transmission parts widely used in marine projects such as ship's main engines, auxiliary engines, offshore platforms, deep sea winches, and subsea compressors due to their high bearing capacity and wear resistance. However, the sliding bearing wears under heavy load, lack of lubricating oil, or long-term operation, which affects their life. Therefore, it is imperative to study the tribological properties of sliding bearings, explore methods for evaluating these properties, and explore the wear mechanism, to ensure the development of marine engineering [1–3].

Multiple scholars have carried out studies on the tribological properties of sliding bearings. Li et al. [4] used the sliding bearing as the supporting bearing for the high-speed rolling bearing test rig for the purpose of prolonging the service life, increasing the load capacity, and promoting the operating stability. Chen et al. [5] used the time-domain numerical integration method to study the influence of factors such as fit clearance, rotor unbalance, and bearing outer ring tightening torque on the vibration response. The bearing fit clearance fault test was performed to verify the simulation results. Chiang et al. [6] developed dynamic models of the pump rotor-bearing systems, including gyroscopic moments, rotary inertias, and bending and shear deformations. The models were analyzed in order to predict the natural frequencies, produce critical speed maps, and estimate the bearing stiffness. Lin et al. [7] reviewed the advantages of replacing the mechanical bearings of low-temperature pumps with radial high-temperature superconductor (HTS)

bearings. Zeng et al. [8] studied the characteristics of the flow and pressure in the axletree room by a computed fluid dynamics method for the abrasion of the axletree. Analysis showed that the reason for the abrasion and high heat generation rate of the axletree was cavitation; the cavitation was caused by the flow acceleration effect of the local area. Iwata et al. [9] used a bearing tester that was certified by the International Organization for Standardization to reproduce the sliding behavior occurring between the crank journal and main bearings in actual engines. Henry et al. [10] developed an experimental approach to analyze the behavior of different types of thrust bearings with fixed geometry. They mainly focused on the capability of textured thrust bearings to lift up during start-up. Jang et al. [11] developed an analytical model to study an unloaded journal bearing. This model consisted of two concentric cylinders containing lubricant, where the inner one rotated at a specified rpm, and the outer one was stationary. The appropriate governing equations and numerical solution schemes for treating the transient heat transfer in the fluid and the bounding solids were then presented. Pathak et al. [12] investigated the antiseizure and antifriction characteristics of a number of AI-Si-Pb alloys with silicon contents in the range of 2–20 wt.% and lead contents in the range of 0–10 wt.% under different lubrication conditions using a bearing test machine. Li et al. [13] calculated the pressure of the oil film with surface roughness and introduced the generalized Reynolds equation of the average flow model. The oil film temperature control equation and the bearing heat conduction equation were used to calculate the bearing temperature. In this setting, the Reynolds equation, temperature control equation, and journal motion equation were combined to establish the transient thermoelastic fluid lubrication analysis model of journal bearings. To establish the calculation model of the hydrodynamic sliding bearing, Luo et al. [14] considered the conservation equation in the flow field of the sliding bearing under the boundary condition when the oil film breaks and subsequently applied the finite volume method to calculate the fluid character. Xie et al. [15] analyzed the relationship between bearing and coaxial neck rotation speed based on the computational fluid dynamics analysis of sliding bearing oil film and established an oil film finite element model. The variations of the oil film pressure, the bearing capacity, the oil film component distribution, and the bearing bush stress and strain were analyzed under the condition of journal speed variation. Gerzos et al. [16] used semi-Sommerfeld conditions as boundary conditions and obtained the lubrication state of non-Newtonian fluid and the static characteristics of bearings lubricated, using Newtonian fluid, by solving the N–S basic equation. Song et al. [17] found that the bearing capacity of oil film was inversely proportional to the gas holdup value at high speed. In order to reduce the influence of cavitation, the increase in oil supply pressure and the decrease in oil film thickness can be used.

Although multiple scholars have studied the tribological properties of sliding bearings, their work has always cut sliding bearings into small samples, which is far from reality. Moreover, the calculation is always separate from experimentation, and the wear mechanism of the sliding bearing is still ambiguous. In this study, a simulation model is established, and a component-level tribological test machine is designed to investigate the tribological properties of the sliding bearing by calculation and experiment. Furthermore, the wear mechanism is analyzed through the wear test. This study aims to provide theoretical guidance for the friction durability and life prediction of sliding bearings used in marine engineering.

2. Simulation Model

2.1. Assumption

The Fortran language was used to calculate the lubrication and force of the sliding bearing. The assumptions of the model are as follows:

(1) The body force of the lubricating fluid is ignored;
(2) It is modified. The lubricating fluid does not slide on the interface, that is, the relative velocity between the interface fluid and the surface is zero;

(3) The fluid pressure and viscosity remain unchanged in the thickness direction of the lubricating oil film;
(4) The thickness of the lubricating oil film is much smaller than the radius of curvature of the surface of the friction pair, so the influence of the oil film curvature is ignored;
(5) The flow is laminar, and there is no turbulence in the lubricating oil film;
(6) The inertial force of the lubricating fluid is ignored.

2.2. Average Reynolds Equation

The average Reynolds equation was used to characterize the rough surface via a statistical method. Afterward, the Reynolds equation was modified by the flow factor to consider the influence of the rough surface on lubrication. The governing equation is [18,19]:

$$\frac{\partial}{\partial x}(\phi_x \frac{\rho h^3}{u}\frac{\partial \overline{P}}{\partial x}) + \frac{\partial}{\partial y}(\phi_y \frac{\rho h^3}{u}\frac{\partial \overline{P}}{\partial y}) = 6U\rho\phi_c \frac{\partial h}{\partial x} + 6U\sigma \frac{\partial(\rho\phi_s)}{\partial x} + 12\rho\phi_c \frac{\partial h}{\partial t} \quad (1)$$

where h is the nominal lubricant film thickness, σ the root mean square of surface roughness, ϕx and ϕy are the pressure flow factors, ϕs denotes the shear flow factor, and ϕc represents the dimensionless contact factor. The pressure flow factor and shear flow factor are functions of the root mean square of surface roughness, surface orientation parameters, and lubricating oil film thickness obtained through local lubrication numerical analysis experiments. The dimensionless contact factor is a function of the root mean square of surface roughness and lubricating oil film thickness and is related to the way the surface roughness is distributed.

2.3. Oil Film Geometric Equation

(1) Nominal oil film thickness

The nominal oil film thickness refers to the oil film thickness between the two surfaces of the shaft and the bearing bush without considering the surface's roughness. Its expression is:

$$h = h_0 + h_x + h_y \quad (2)$$

where h_0 is the minimum oil film thickness between the lubricating surfaces of the bearing bush and the shaft. This is a critical parameter, which is often adjusted in the calculation to make the calculation results converge; h_x and h_y represent the incremental value of the bearing oil film thickness in the x- and y- directions, respectively.

(2) Actual oil film thickness

Due to the limitations of processing and manufacturing technology, as well as processing accuracy, it is impossible to process the sliding bearing and shaft with an absolutely smooth surface, so a certain roughness does exist on both surfaces of the bearing. Moreover, for multiple high-power internal combustion engines, the sliding bearing needs to bear a large alternating load. At this time, the oil film pressure of the bearing is significantly large, and the minimum oil film thickness of the bearing is extremely small, the roughness peak value of the bearing surface and the minimum oil film thickness value are almost of the same order of magnitude, and the bearing surface often produces contact with rough peaks. Thus, the surface morphology of the bearing has a major impact on the lubricating characteristics of the bearing. Therefore, the actual factors such as surface roughness and rough surface profile must be taken into account when carrying out the analysis of the bearing lubrication performance.

The force on the bearing surface generates elastic deformation, which causes the thickness of the oil film to change. Furthermore, the actual bearing surface is rough, and the surface morphology—especially the peaks and valleys—also causes changes in the thickness of the bearing oil film. In summary, when the bearing surface roughness and elastic deformation factors are taken into account, the calculated oil film thickness becomes the actual oil film thickness, which is expressed as:

$$h_T = h + \delta_1 + \delta_2 \tag{3}$$

where h is the nominal oil film thickness, δ_1 and δ_2 represent the random roughness height of the shaft and bearing surface, respectively, and the elastic deformation is negligible.

(3) Lubricating oil viscosity

In the numerical analysis of lubrication, the viscosity-temperature and viscosity-pressure characteristics of the lubricating oil are the influencing factors to be considered. The change in oil viscosity with temperature is a critical characteristic of oil. Lubricating oil viscosity is a macroscopic manifestation of the momentum and gravitational effects between the molecules inside the lubricating oil. When the temperature increases, the average velocity of the fluid molecules augments, and the momentum increases; the distance between the molecules increases while the force between the molecules decreases. Generally, the viscosity of liquids diminishes rapidly with increasing temperatures, while the viscosity of gases increases slightly with increasing temperatures. Moreover, the change in oil viscosity with pressure is a major characteristic of oil. When the pressure on the fluid increases, the distance between the fluid molecules decreases, the interaction force augments, and the viscosity increases. This study adopts the Roeland viscosity model [20,21].

$$u = u_0 \exp\left\{\left(\ln u_0 + 9.67\right)\left[\left(1 + 5.1\times10^{-9}\, p\right)^{Z} \times \left(\frac{\mathrm{T}-138}{\mathrm{T}_0 - 138}\right)^{-S} - 1\right]\right\} \tag{4}$$

where T_0 is the reference temperature, T is the actual temperature, u_0 is the viscosity at T_0, p is the actual pressure of the lubricating oil, Z is the viscosity-pressure index, and S is the viscosity-temperature index.

(4) Flow factor

The formula for calculating the pressure flow factor is as follows [18]:

$$\begin{cases} \phi_x = 1.0 - Ce^{-rH} & \gamma \le 1 \\ \phi_x = 1.0 + Ce^{-rH} & \gamma > 1 \end{cases} \tag{5}$$
$$\phi_y(1,\gamma) = \phi_x(\lambda, 1/\gamma)$$

where C and r are constants. ϕx and ϕy represent the pressure flow factors in the x- and y- directions, respectively. γ indicates the direction of bearing surface roughness: when γ is superior to 1, it means longitudinal rough stripes; when γ is inferior to 1, it means transverse rough stripes; and when γ is equal to 1, it means isotropic rough stripes. However, generally, γ is set to 1.

The formula for calculating the shear flow factor is as follows [19]:

$$\phi_s = \left(\frac{\delta_1}{\delta}\right)^2 \Phi_s(H, \gamma_1) - \left(\frac{\delta_2}{\delta}\right)^2 \Phi_s(H, \gamma_2) \tag{6}$$

where δ_1 and δ_2 represent the random roughness height of the shaft and bearing surface, respectively. γ_1 and γ_2 denote the grain direction parameters of the surface roughness of the shaft and bearing, respectively. Φ_S is calculated as follows:

$$\begin{cases} \Phi_s = A_1 H^a e^{-bH + cH^2} & H \le 5 \\ \Phi_s = A_2 e^{-bH} & H > 5 \end{cases} \tag{7}$$

where A_1, A_2, a, b, and c are constants.

2.4. Rough Contact Model

When the lubricating oil film is very thin, the asperities on the two rough surfaces of the bearing and journal will contact and interact with each other, which will have a certain impact on the lubricating performance of the lubricating surface. Greenwood and Tripp [22] established a roughness contact model to study the contact behavior of micro convex

bodies. In this model, the probability density functions of various contact surface roughness height distributions are considered. When the probability density function of the roughness height distribution of two contact surfaces is a normal Gaussian distribution with a mean value equal to zero, the calculation expressions of the contact force between the asperities on the rough surface and the actual contact area of the rough surface are as follows:

$$p_{asp} = \frac{16\sqrt{2}}{15}\pi(\eta\beta\delta)^2 E' \sqrt{\frac{\sigma}{\beta}} F_{2.5}(H) \tag{8}$$

$$A_c = \pi^2(\eta\beta\delta)^2 A F_2(H) \tag{9}$$

$$E' = \frac{1}{\frac{1-v_1^2}{E_1} + \frac{1-v_2^2}{E_2}} \tag{10}$$

$$F_2(H) = \begin{cases} 1.705 * 10^{-4} \exp(4.05419 \ln(4.0 - H) + 1.37025(\ln(4.0 - H))^2) & H \le 3.5 \\ 8.8123 * 10^{-5} (4.0 - H)^{2.1523} & 3.5 < H \le 4 \\ 0 \quad H > 4 \end{cases} \tag{11}$$

$$F_{2.5}(H) = \begin{cases} 2.1339 * 10^{-4} \exp(3.804467 \ln(4.0 - H) + 1.341516(\ln(4.0 - H))^2) & H \le 3.5 \\ 1.1201 * 10^{-4} (4.0 - H)^{1.9447} & 3.5 < H \le 4 \\ 0 \quad H > 4 \end{cases} \tag{12}$$

where p_{asp} is the contact pressure of the rough asperity, A_c is the actual contact area of the rough surface, A is the nominal contact area, η and β are the contact parameters, E_1 and E_2 are the elastic moduli of the bearing bush and shaft, respectively, E' is the comprehensive elastic modulus, and v_1 and v_2 are the Poisson's ratio of the bearing bush and shaft, respectively. Moreover, $F_2(H)$ and $F_{2.5}(H)$ are calculated by an empirical formula. H is the film thickness ratio.

2.5. Friction

The roughness of the shaft and the bearing bush affect the lubrication's performance. Under the steady-state load and the linear speed of the calibration condition, the friction mainly includes the rough contact friction and the fluid lubrication friction.

$$F_T = F_C + F_V = \iint_A (\tau_C + \tau_V) dxdz \tag{13}$$

where τ_c is the rough contact shear stress and τ_v is the fluid lubrication shear stress.

2.6. Boundary Conditions

The boundary conditions are as follows:

$$\begin{gathered} \frac{\partial p}{\partial y} \Big|_{y=-\frac{d}{2}} = \frac{\partial p}{\partial y} \Big|_{y=\frac{d}{2}} = 0 \\ p(x, -\frac{l}{2}) = p(x, \frac{l}{2}) = 0 \end{gathered} \tag{14}$$

where the x-direction represents the axial direction, and the y-direction represents the radial direction. d represents the diameter of the sliding bearing, and l denotes the width of the sliding bearing.

2.7. Calculation Process

The calculation process is shown in Figure 1. The program is based on the Fortran language. Firstly, each parameter of the model's design is put into the calculation program, the load is applied to calculate the pressure on the sliding bearing, and the initial oil film thickness can be obtained at each position given the minimum oil film thickness. Secondly, the finite difference method is used to solve the average Reynolds equation, the over-relaxation iterative method is used to predict the thickness of the oil film gradually approaching the real, and the radial force of the sliding bearing is calculated to determine whether the radial load is balanced. Hence, if it is not balanced, correct the initial oil film thickness, and return to the step of solving the Reynolds equation. Recalculate according to the steps until the balance is reached, and subsequently proceed to the next step to judge whether the oil film thickness is converged. If it does not converge, go back to the beginning of the loop, and recalculate according to the steps until the result is output after convergence and the program ends. The rough peak contact friction and fluid lubrication friction between the bearing and journal can be obtained by solving the average Reynolds equation, and the friction under corresponding working conditions can be obtained by summing them. The value of calculation parameters are listed in Table A1 of Appendix A.

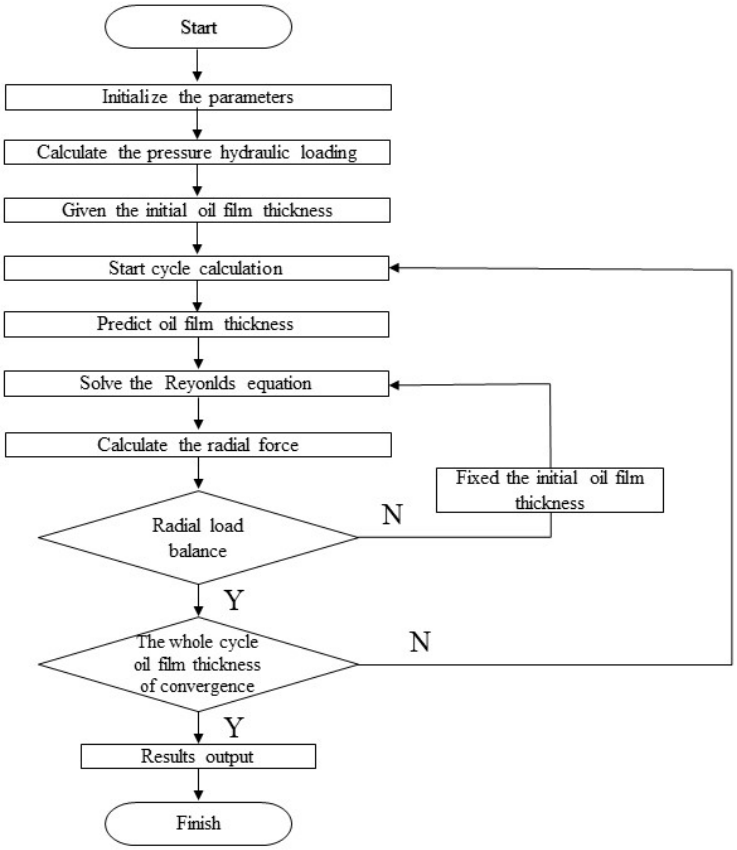

Figure 1. Calculation process.

3. Experimental Details

The component-level tribological test machine is shown in Figure 2. In the test, the sliding bearing was fixed and the straight shaft rotated under the drive of the motors, which provided the guarantee of the movement speed and the wear stroke for the relative friction movement of the shaft and the sliding bearing. The pressure is transmitted to the shaft along the vertical direction, providing a strengthened load to accelerate the wear. Moreover, an oil pipe was arranged below the bearing seat for the lubricating oil supply, forming an oil film between the shaft and the bearing. The friction force data was real-

time collected by the sensor. The sliding bearing before testing is shown in Figure 3, while the structure diagram is shown in Figure 4. The sliding bearing is formed of steel, aluminum alloy, nickel, and PbSn18Cu2.

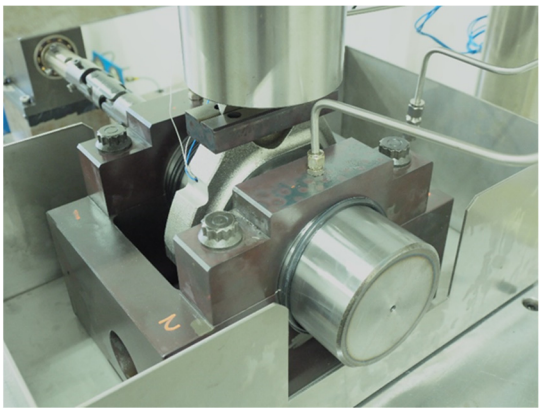

Figure 2. The component-level tribological test machine.

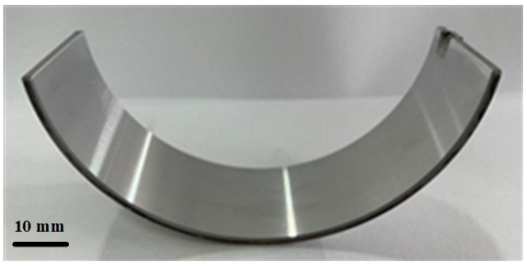

Figure 3. Sliding bearing.

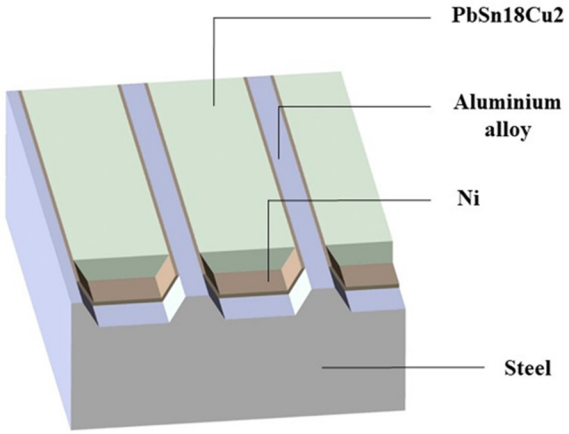

Figure 4. Structure diagram of the sliding bearing.

The wear test parameter is listed in Table 1. The sliding bearing bush is in the hydrodynamic lubrication state under normal working conditions, so it is difficult to wear. Therefore, in order to wear the bearing bush in a short time, appropriate working condition parameters are required to make the bearing bush in mixed lubrication or boundary lubrication state. The operating condition parameters are determined through a large number of tests. The speed is selected as 100 r/min, so that hydrodynamic lubrication cannot be formed. The operating temperature of the lubricating oil of the actual diesel engine is selected as the oil temperature, and the load is selected as 2 t and 3 t. Under this condition, the bearing pads will be worn after a certain period of wear. Therefore, the operating condition parameters are selected.

Table 1. Condition parameters.

Case	Load	Speed	Oil Temperature	Time
Case 1	2 t	100 r/min	90 °C	24 h
Case 2	3 t	100 r/min	90 °C	24 h

4. Validation

Two working conditions (Case 1 and Case 2) were selected to compare the calculated friction obtained by the simulation model and the measured friction acquired by the experiment. The loads of Case1 and Case2 are 2 tons and 3 tons, respectively, and the other parameters are the same. The measured friction is obtained during the period of normal operation. The comparison of the calculated average friction and the measured average friction is shown in Figure 5. The errors between the calculated average friction and the measured average friction are within 10% in two cases. Thus, verifying the simulation model is feasible.

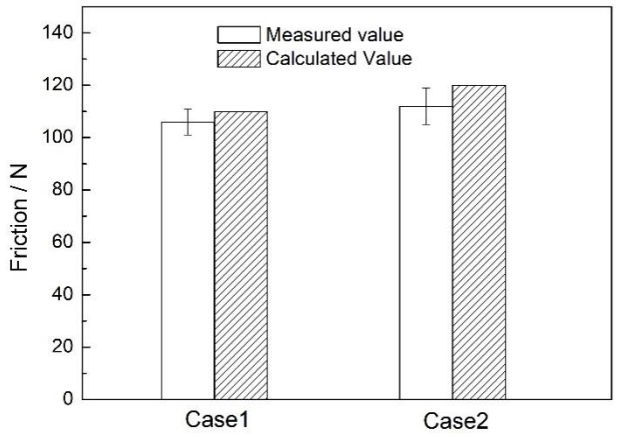

Figure 5. Comparison of the calculated average friction and the measured average friction.

5. Experimental Results and Mechanisms

5.1. Wear Loss

An analysis balance (Mettler Toledo, Swiss) with an accuracy of 0.1 mg was used to calculate the varied weight of the bushing before and after tests. Figure 6 shows the wear loss for 24 h under the conditions of Case 1 and Case 2, and the wear amount is measured every 3 h. It is clear from the figure that with the increase in wear time, the wear amount is augmenting. In the beginning, the wear amount increases rapidly due to the fact that the wear rate is large, and after 21 h for Case 1 and 18 h for Case 2, the wear amount becomes flat. At the start, the asperities on the surface of the sliding bearing and the shaft surface are in contact with each other, and after a period of running-in, the asperities are gradually smoothed, so the initial wear amount is large. After reaching a certain running-in balance state, with the increase in time, the wear amount tends to become gentle.

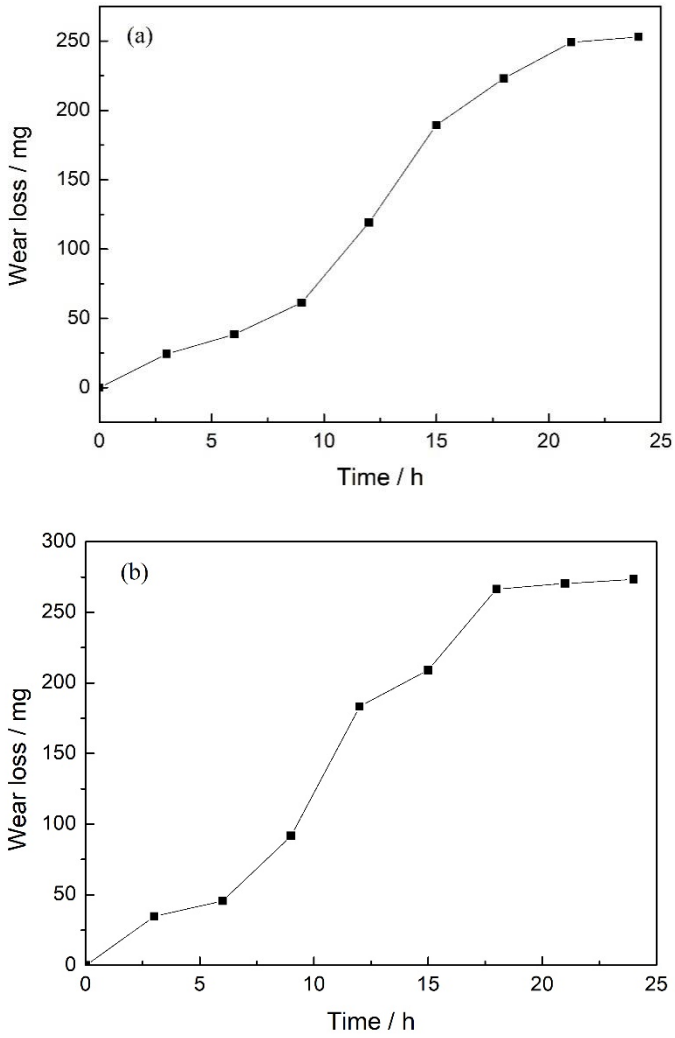

Figure 6. Wear loss of sliding bearing along with time. (**a**) Case 1 and (**b**) Case 2.

5.2. Wear Mechanisms

Philips-30 TMP scanning electron microscope with the energy dispersive X-ray spectrometer is used to investigate the surface and element. Figure 7 shows the original surface morphology and element distribution of the sliding bearing. The groove shape is clear, and the element distribution is uniform. The narrower part in the figure is the aluminum alloy, while the wider part is PbSn18Cu2. The overall surface is flat. Along the circumferential direction, there are clear marks of machining.

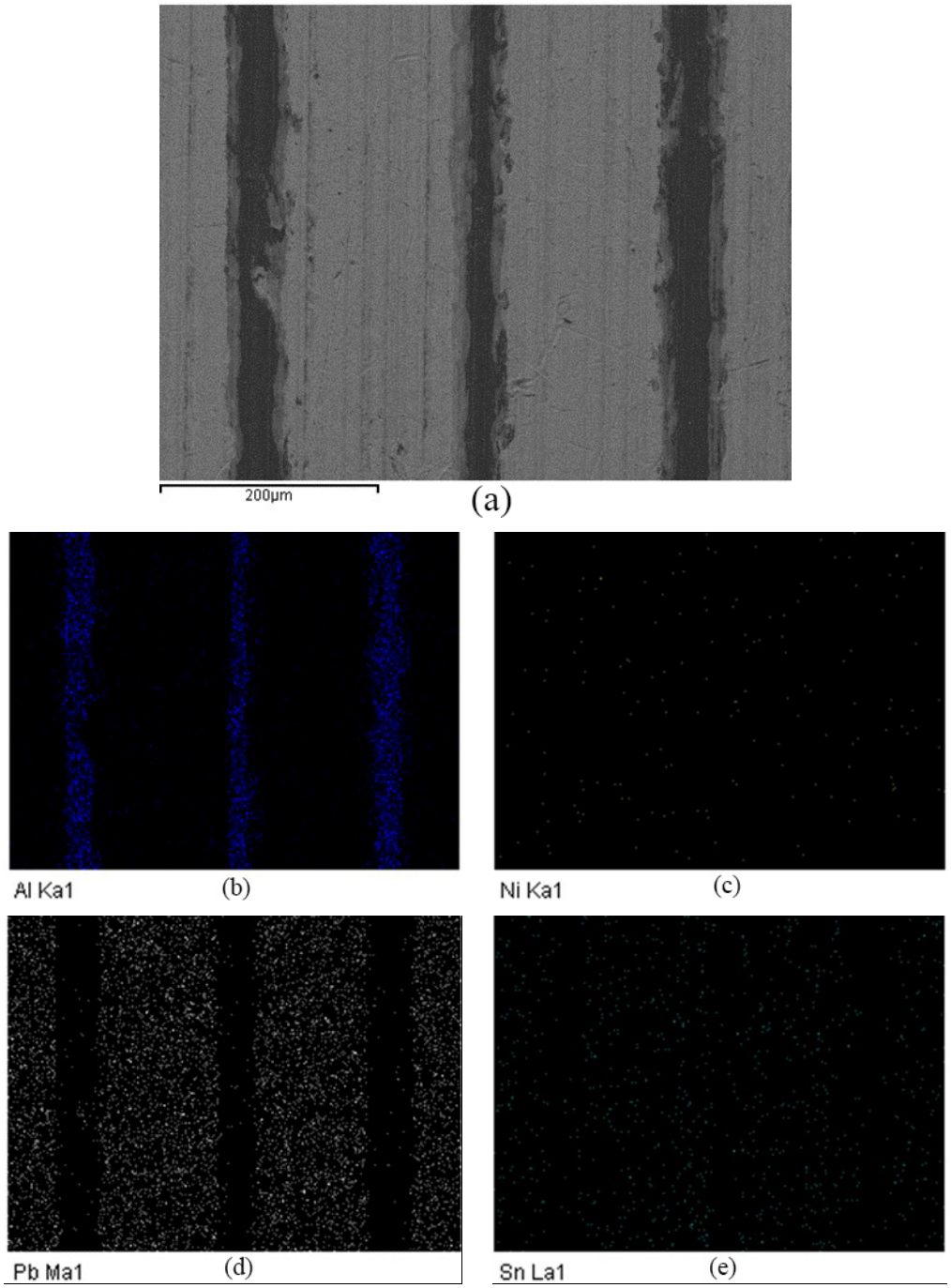

Figure 7. Original surface morphology and element distribution of the sliding bearing. (**a**) Surface morphology, (**b**) Al distribution, (**c**) Ni distribution, (**d**) Pb distribution, (**e**) and Sn distribution.

Figure 8 shows the surface micromorphology and element distribution after 24 h of wear. The surface coating is extruded and deformed, the edge of the coating is broken, and plastic rheology occurs simultaneously, which is attached to the surface of the aluminum alloy. There are visible scratches along the sliding direction.

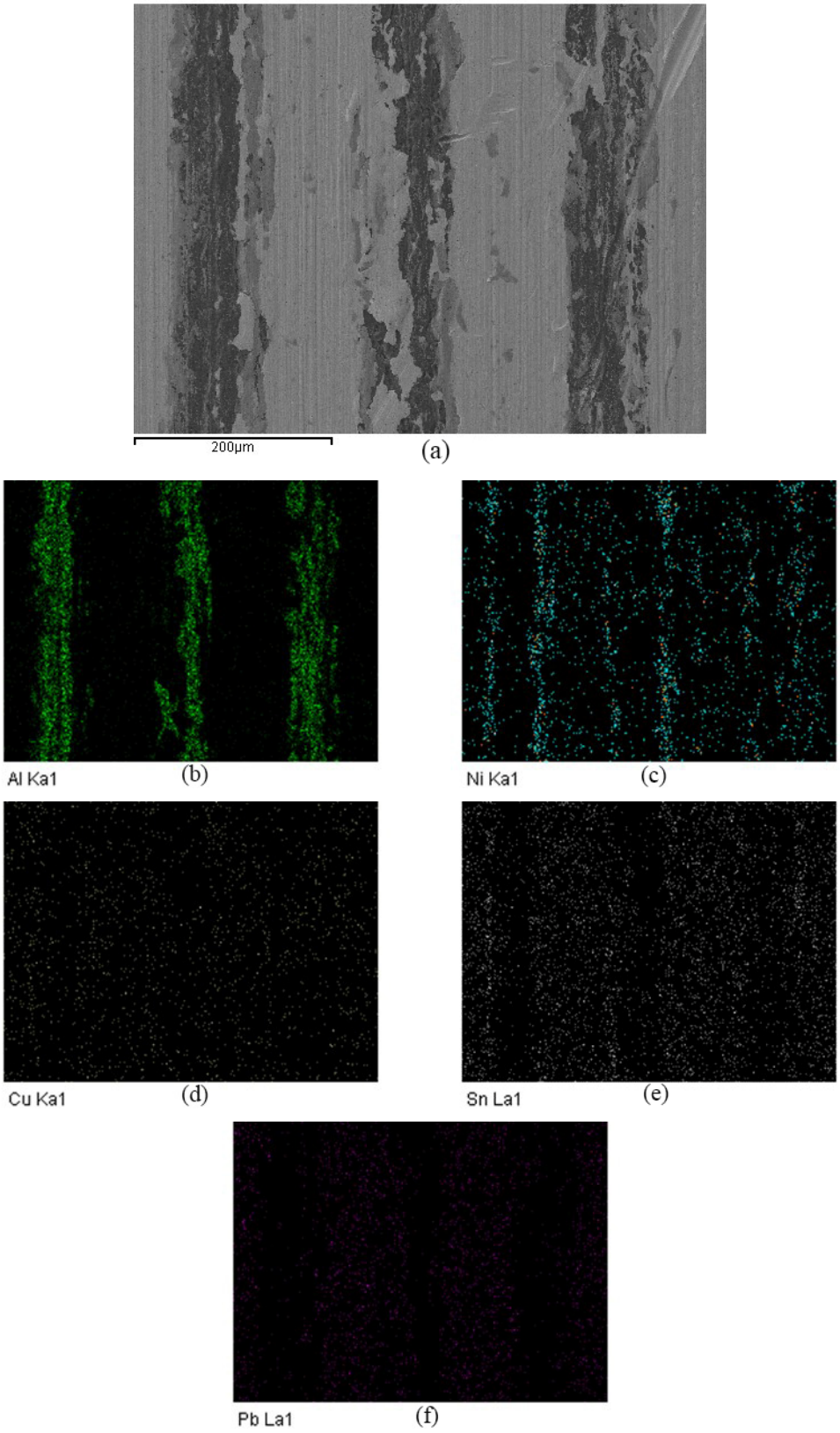

Figure 8. Surface morphology and element distribution of the sliding bearing after wear. (**a**) Surface morphology, (**b**) Al distribution, (**c**) Ni distribution, (**d**) Cu distribution, (**e**) Sn distribution, and (**f**) Pb distribution.

Figure 9 shows the wear mechanism. Figure 9a is the original state of the sliding bearing. The aluminum alloy is combined with the steel back, there exists a groove structure on the surface of the aluminum alloy, and the nickel grid and PbSn18Cu2 ternary alloy are electroplated in the groove. The layers are well combined, and the surface coating is flat and evenly distributed. Figure 9b shows the wear mechanism of the sliding bearing. After wear, the groove structure remains, and the sliding bearing shows a trend of gradually thinning the surface. The height of the groove boss decreases, and the cross-sectional area becomes slightly wider. Under the rotational shearing action of the shaft and the sliding bearing, the ternary alloy in the groove will be taken out of the groove with the rotation of the shaft, and its edge will undergo plastic flow and adhere to the surface of the aluminum alloy boss.

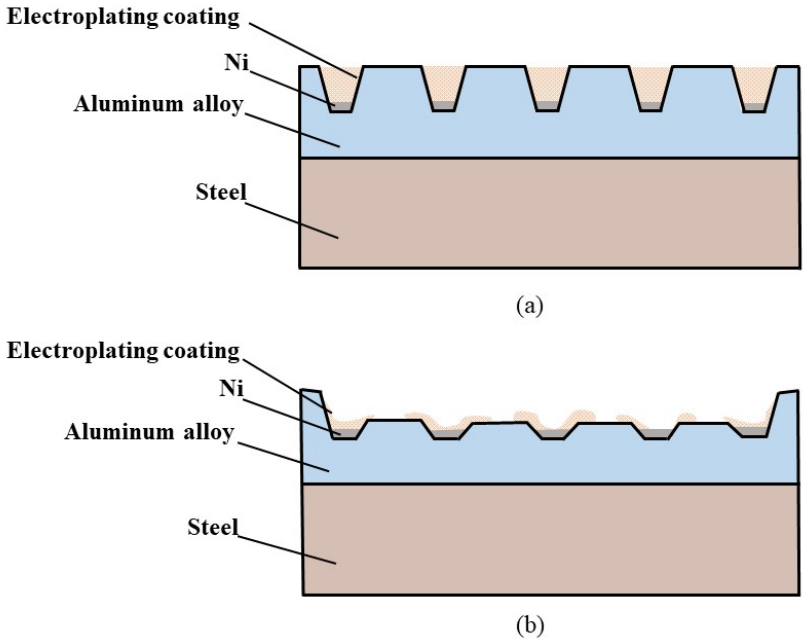

Figure 9. Wear mechanism of the sliding bearing. (**a**) Original (**b**) and after wear.

6. Conclusions

In this study, the simulation and experiment are combined to investigate the wear failure of the sliding bearing. The method could provide theoretical guidance for the friction durability of sliding bearings used in marine engineering. The main conclusions are as follows:

(1) The errors between the calculated average friction and the measured average friction are within 10%, which proves the correctness of the simulation model.
(2) Through 24 wear tests, the wear loss of the sliding bearing is larger at the initial stage because the asperities on the surface of the sliding bearing and the shaft surface are in contact with each other, and it tends to become gentle after the running-in period.
(3) After wear, the groove structure remains, the height of the groove boss decreases, and the cross-sectional area becomes slightly wider. The ternary alloy in the groove will be taken out of the groove, and its edge will undergo plastic flow and adhere to the surface of the aluminum alloy. The research on the wear mechanism can provide guidance for the improvement of wear resistance technology.

Author Contributions: Data curation, D.L., M.H., Y.Y.; methodology, W.W.; writing—original draft, F.D. All authors have read and agreed to the published version of the manuscript.

Funding: This research was supported by the Dalian High-level Talents Innovation Support Program (2020RQ129).

Institutional Review Board Statement: Not applicable.

Informed Consent Statement: Not applicable.

Data Availability Statement: Not applicable.

Conflicts of Interest: The authors declare no conflict of interest.

Nomenclature

Item	Meaning
h	nominal lubricant film thickness
σ	root mean square of surface roughness
ϕx	the pressure flow factor in the x-direction
ϕy	the pressure flow factor in the y-direction
ϕs	the shear flow facto
ϕc	the dimensionless contact factor
h	the nominal oil film thickness
u	the actual viscosity
t	time
h_0	the minimum oil film thickness
h_x	the incremental value of the bearing oil film thickness in the x-direction
h_y	the incremental value of the bearing oil film thickness in the y-direction
h_T	the actual oil film thickness
δ_1	the random roughness height of the shaft
δ_2	the random roughness height of the bearing surface
T_0	the reference temperature
T	the actual temperature
u_0	the viscosity at T_0
p	the actual pressure of the lubricating oil
Z	the viscosity-pressure index
S	the viscosity-temperature index
γ	the direction of bearing surface roughness
γ_1	the grain direction parameters of the surface roughness of the shaft
γ_2	the grain direction parameters of the surface roughness of the bearing
p_{asp}	the contact pressure of the rough asperity
A_c	the actual contact area of the rough surface
A	the nominal contact area
E_1	the elastic modulus of bearing bush
E_2	the elastic modulus of shaft
E′	the comprehensive elastic modulus
v_1	the Poisson's ratio of the bearing bush
v_2	the Poisson's ratio of the shaft
H	the film thickness ratio
F_c	the rough contact friction
F_v	the fluid lubrication friction
τ_c	the rough contact shear stress
τ_v	the fluid lubrication shear stress
x	the axial direction
y	the radial direction
d	the diameter of the sliding bearing
l	the width of the sliding bearing

Appendix A

Table A1. The value of calculation parameters.

Item	Value
h_0	10 μm
δ_1	0.8 μm
δ_2	0.8 μm
E_1	1.7×10^{11} Pa
E_2	2×10^{11} Pa
v_1	0.25
v_2	0.29
d	100 mm
l	30 mm
Load	2,3 tons
Speed	100 r/min
Oil temperature	90 °C
u_0	0.08 Pa·s
S	1.1
Z	0.68
T_0	25 °C
T	90 °C
γ_1	1
γ_2	1
A_1	1.899
A_2	1.126
a	0.98
b	−0.92
c	0.05

References

1. Zhu, J.X.; Li, H.C.; Wei, S.J.; Fu, J.F.; Xu, X. An approach of simulating journal bearings-gear pump system including components' cavitation. *Simulaiton Model. Pract. Theory* **2021**, *108*, 102236. https://doi.org/10.1016/j.simpat.2020.102236.
2. Yang, C.Y.; Wang, S.J.; Lin, C.K.; Chung, L.L.; Liou, M.C. Analytical and experimental study on sloped sliding-type bearings. *Struct. Control Health Monit.* **2021**, *28*, e2828. https://doi.org/10.1002/stc.2828.
3. Brenkacz, L.; Witanowski, L.; Drosinska-Komor, M.; Szewczuk-Krypa, N. Research and applications of active bearings: A state-of-the-art review. *Mech. Syst. Signal Process.* **2021**, *151*, 107423. https://doi.org/10.1016/j.ymssp.2020.107423.
4. Li, H.; Liu, H.; Qi, S.M.; Liu, Y. A high-speed rolling bearing test rig supported by sliding bearing. *Ind. Lubr. Tribol.* **2020**, *72*, 955–959. https://doi.org/10.1108/ILT-03-2020-0085.
5. Chen, G.; Qu, M.J. Modeling and analysis of fit clearance between rolling bearing outer ring and housing. *J. Sound Vib.* **2019**, *438*, 419–440. https://doi.org/10.1016/j.jsv.2017.11.004.
6. Chiang, H.W.D.; Kuan, C.P.; Li, H.L. Turbomolecular pump rotor-bearing system analysis and testing. *J. Vac. Sci. Technol. A* **2009**, *27*, 1196–1203. https://doi.org/10.1116/1.3179157.
7. Lin, Q.X.; Jiang, D.H.; Deng, Z.G.; Ma, G.T.; Zheng, J.; Wang, W.J.; Shin, D.I.; Gu, X.; Lin, N.; Shao, M.L. Operation and improvement of liquid nitrogen pumps with radial high-temperature superconductor bearings. *J. Low Temp. Phys.* **2015**, *180*, 416–424. https://doi.org/10.1007/s10909-015-1321-y.
8. Zeng, X.K.; Zhou, H.H.; Xiong, W.Y. CFD study on cavitation abrasion for axletree of main pump of tianwan NPP. *Nucl. Power Eng.* **2016**, *37*, 4–8. https://doi.org/CNKI:SUN:HDLG.0.2016-02-032.
9. Iwata, T.; Oikawa, M.; Chida, R.; Ishii, D.; Ogihara, H.; Mihara, Y.; Kano, M. Excellent seizure and friction properties achieved with a combination of an a-C:H:Si DLC-coated journal and an aluminum alloy plain bearing. *Coatings* **2021**, *11*, 1055. https://doi.org/10.3390/coatings11091055.
10. Henry, Y.; Bouyer, J.; Fillon, M. Experimental analysis of the hydrodynamic effect during start-up of fixed geometry thrust bearings. *Tribol. Int.* **2018**, *120*, 299–308. https://doi.org/10.1016/j.triboint.2017.12.021.
11. Jang, J.Y.; Khonsari, M.M.; Pascovici, M.D. Modeling aspects of a rate-controlled seizure in an unloaded journal bearing. *Tribol. Trans.* **1998**, *41*, 481–488. https://doi.org/10.1080/10402009808983772.

12. Pathak, J.P.; Torabian, H.; Tiwari, S.N. Antiseizure and antifriction characteristics of Al-Si-Pb alloys. *Wear* **1997**, *202*, 134–141. https://doi.org/10.1016/S0043-1648(96)07241-9.
13. Li, S. *Transient Coupling Study of Dynamics and Tribology on Sliding Bearing*; Harbin Engineering University: Harbin, China, 2017.
14. Luo, Z. *Analysis of Fluid-Structure Interaction Heat Transfer of Hydrodynamic Journal Bearing Considering Thermohydrodynamic*; Xiangtan University: Xiangtan, China, 2016.
15. Xie, Y.; Zhang, B.; Hu, Y.M.; Ruan, D.F. Effect of journal rotation speed on characteristic of oil film and structure characteristic of bearings. *Lubr. Eng.* **2015**, *40*, 8–16. https://doi.org/10.3969/j.issn.0254-0150.2015.11.005.
16. Gertzos, K.P.; Nikolakopoulos, P.G.; Papadopoulos, C.A. CFD analysis of journal bearing hydrodynamic lubrication by Bingham lubricant. *Tribol. Int.* **2008**, *41*, 1190–1204. https://doi.org/10.1016/j.triboint.2008.03.002.
17. Song, Y.; Ren, X.; Gu, C.W. Experimental and numerical studies of cavitation effects in a tapered land thrust bearing. *J. Tribol.* **2015**, *137*, 011701. https://doi.org/10.1115/1.4028264.
18. Patir, N.; Cheng, H.S. An average flow model for determining effects of three-dimensional roughness on partial hydrodynamic lubrication. *J. Lubr. Technol.* **1978**, *100*, 12–17. https://doi.org/10.1115/1.3453103.
19. Parir, N.; Cheng, H.S. Application of average flow model to lubrication between rough sliding surfaces. *J. Lubr. Technol.* **1979**, *101*, 220–230. https://doi.org/10.1115/1.3453329.
20. Houpert, L. New results of traction force calculations in elastohydrodynamic contacts. *J. Tribol.* **1985**, *107*, 241–245. https://doi.org/10.1115/1.3261033.
21. Wang, S.; Cusano, C.; Conry, T. Thermal analysis of elastohydrodynamic lubrication of line contacts using the Ree-Eyring fluid model. *J. Tribol.* **1991**, *113*, 232–242. https://doi.org/10.1115/1.2920611.
22. Greenwood, J.A.; Tripp, J.H. The Contact of Two Nominally Flat Surfaces. *Proc. Inst. Mech. Eng. Part J J. Eng. Tribol.* **1971**, *185*, 625–633. https://doi.org/10.1243/PIME_PROC_1970_185_069_02.